Exogenous Amyloid Sequences: Their Role in Amyloid-Beta Heterotypic Aggregation

Jofre Seira Curto[1], Sandra Villegas Hernandez[1], Maria Rosario Fernandez[1], Natalia Sanchez de Groot[1]*
[1]Unitat de Bioquímica. Departament de Bioquímica i Biologia Molecular. Universitat Autònoma de Barcelona, Spain.

*** Correspondence:**
Corresponding Author
natalia.sanchez@uab.cat
jofre.seira@uab.cat

Keywords: microbiome, Alzheimer's, aggregation, amyloid.

Abstract
Protein aggregation is a complex process influenced by environmental conditions and interactions between multiple molecules, including those of exogenous origin. Although *in vitro* simulations of aggregation are crucial for advancing research, few studies explore cross-seeding as a repeating event, despite the potential for such events when proteins circulate through the body. Here, we investigated the impact of exogenous amyloid sequences derived from the gut microbiota on the heterotypic aggregation of Aβ peptides. We utilized ten 21-amino acid peptides derived from bacterial genomes, previously shown to interfere with Aβ40 aggregation and induce memory loss in *Caenorhabditis elegans*. Through consecutive cross-seeding assays with Aβ40 and Aβ42, we analyzed the effects of these peptides on aggregation kinetics and seed propagation. Our findings indicate that exogenous molecules can influence Aβ's aggregation process, altering the fibrils' properties. Based on this, we introduce the "Interaction History" concept, where prior interactions shape the aggregation and propagation of Aβ peptides. This work supports the idea that environmental factors, such as microbial amyloids, can contribute to the heterogeneity and progression of amyloid-related diseases. Our results highlight the need for therapeutic strategies targeting diverse amyloid configurations and underscore the importance of considering exogenous sequences as additional triggers in AD pathology.

Introduction
Protein aggregation is associated with many neurodegenerative diseases. In particular, the formation of amyloid plaques has been widely described in the brains of Alzheimer's disease (AD) patients[2–6]. These deposits are composed principally of amyloid beta peptide (Aβ), which exist in two major isoforms: Aβ40, the most abundant in the body, and Aβ42, the main component of amyloid plaques [5,7] (Figure 1A). These two isoforms, differ in length and aggregation propensity and can interact with each other, producing different outcomes[3,8–12]. For instance, *in vivo* studies have shown that Aβ40 overexpression inhibits Aβ42 deposition, suggesting a potential protective role for Aβ40 [10,13,14]. The balance between Aβ40 and Aβ42 is influenced by isoforms of the apolipoprotein E gene (APOE). Among these, APOE4 is particularly significant, as it promotes Aβ42 formation, exacerbating aggregation and

accelerating disease progression[6,15]. At the molecular level, interlaced amyloid fibrils containing both Aβ40 and Aβ42 have been observed, supporting that these isoforms can interact during the aggregation process [10]. Similarly, compositional analyses of amyloid plaques extracted from patients' brains also revealed heterogeneous aggregation events[16,17]. Notably, emerging evidence suggests that Aβ peptides can cross-seed and propagate aggregation across different regions of the body, potentially contributing to the spread of amyloid pathology[1] (Figure 1A).

Aβ aggregation is not limited to interactions between different isoforms[9,18]; it also involves other proteins, such as amylin[19] or alpha-synuclein[20–22], and non-protein molecules like RNA [23,24] and metals [25–27]. These other molecules, together with changes in local environmental conditions (e.g., pH), can produce amyloid aggregates with distinct structural and biophysical properties [28–30]. These structurally diverse amyloid fibrils, also known as strains, have been linked to different clinical and pathological outcomes in AD[31]. In this line, it has been observed a connection between environmental factors and lifestyle with AD development[32], highlighting the potential impact of exogenous molecules in this process.

Alzheimer's research is gradually expanding to include the microbiota (Figure 1A), which plays a significant role in influencing the host's immune and regulatory processes[33]. In this context, microbiome-derived proteins can be exported and digested, for example, in the gut, resulting in molecules capable of influencing the aggregation of host proteins[33,34]. This aligns with the reported potential of prion-like proteins for transcellular propagation[1] and interspecies transmission[22,35–38]. An increasing body of evidence suggests that microbial cells and their products can circulate through the host body, potentially reaching the brain via the vagus nerve or bloodstream[33,39], thereby able to influencing aggregation processes far away from the original site of infection (Figure 1A).

To investigate the effects of exogenous proteins entering the body, we recently selected and tested a collection of prion-like sequences derived from the gut microbiome[40] (Figure 1B). These sequences have shown the ability to interfere with Aβ40 aggregation *in vitro* and to induce memory loss when ingested by *C. elegans*. In the present study, we aim to investigate how these bacterial sequences influence both the formation of Aβ42 aggregates and, more importantly, the seeding properties of these aggregates, particularly their ability to trigger subsequent aggregation events. We aim to achieve this, giving emphasis to the cross-interactivity between Aβ40 and Aβ42[10] (Figure 1C). We observed that incubating Aβ with bacterial sequences accelerated aggregation and produced deposits with varying seeding capacities (Figures 2-4). These findings suggest that the introduction of additional molecular factors may contribute to protein aggregates diversity, leading to the formation of novel structures and propagation behaviors. This highlights the risk associated with exogenous prion-like proteins or peptides derived from their proteolysis[41,42], as once they enter the body, they can indirectly promote the formation of additional, more toxic aggregated structures (Figure 1A). Therefore, observations of no or low effect in a classical single aggregation kinetic step may be misleading without subsequent aggregation assays (Figure 1C) to assess the seeding capacity of the newly formed aggregates. Overall, our results support that the molecular interactions Aβ experiences during its journey through the body (referred to here as Interaction History, Figure 1C) are critical factors for understanding the disease and developing effective therapeutic approaches.

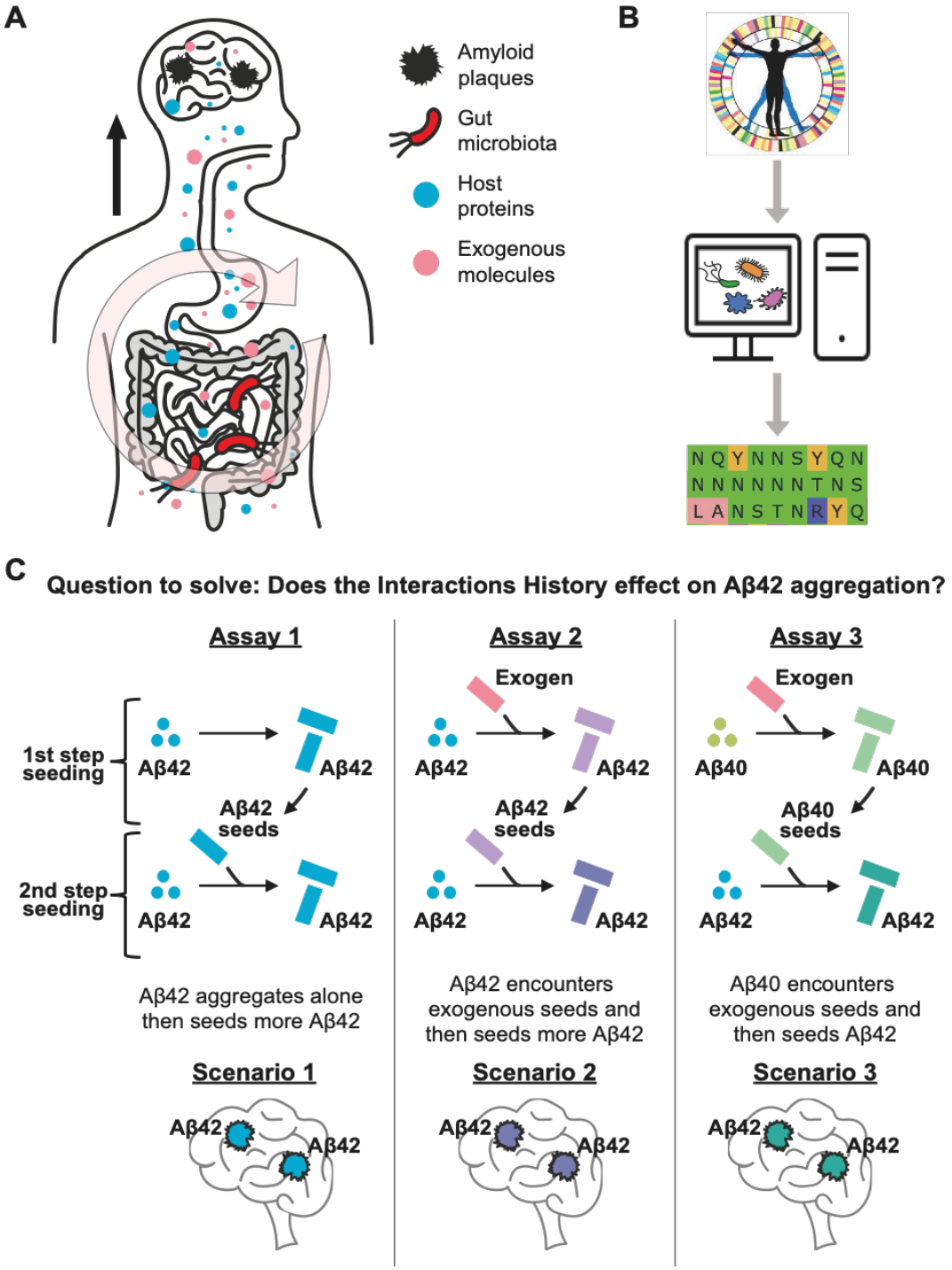

Figure 1. Exogenous Prion-like Sequences Can Affect Aβ Aggregation. *A) Microbial cells and their products can circulate through the body, encountering host proteins, reaching the brain, and influencing aggregation processes. B) We have constructed a set of exogenous prion-like sequences by searching the gut microbiome. C) Interaction History Affects Aβ42 Aggregation. The image illustrates three hypothetical scenarios where two consecutive seeding steps influence Aβ42 aggregation. Scenario 1: Only Aβ42 molecules participate as monomers and seeds in both seeding steps. Scenario 2: Aβ42 aggregates in the presence of an exogenous molecule, and subsequently, these aggregates seed new Aβ42 monomers. Scenario 3: Aβ40*

aggregates in the presence of an exogenous molecule, and subsequently, these Aβ40 aggregates seed Aβ42 monomers.

Results and Discussion

Exogenous Prion-like Sequences Can Influence Aβ Peptides Aggregation

In our previous investigation of the gut microbiome, we developed a collection of exogenous prion-like sequences capable of interfering with Aβ40 aggregation[40] (Figure 1B, Table 1). These sequences were designed based on the amyloid stretch hypothesis, which states that certain sequences within a protein, known as amyloid cores, can drive amyloid nucleation[43–45]. We identified the amyloid cores of the prion-like sequences detected in the gut microbiome and selected 10 of them for our study. Based on the tolerance of prion-like proteins to nucleation domain exchanges[43–45], we incorporated these ten amyloid cores into the yeast prion Sup35 terminator (a well-known prion model), replacing its native nucleation domain. *C. elegans* fed with bacteria expressing these *Sup35* chimeras exhibited memory loss, indicating their potential role in triggering disease in a multicellular organism.

Name	Uniprot ID	Species	Sequences
C1	M5YJZ4	Helicobacter pylori	G N N N N S V I S F N Q T N F N Q G T Y N
C2	M3SJI9	Helicobacter pylori	S S V Y W L N S V N E N N N N K S Y Y I S
C3	C0B555	Coprococcus comes	M Q A A F N F I N N R R Y Q D A I N V L N
C4	C9L6N5	Blautia hansenii	Y Q Q A L N V L S R I Q N R N A Q W Y Y L
C5	D4KZ46	Roseburia intestinalis	H A N E G N V N Q Y N N S Y Q N T N S Y S
C6	C0FUS6	Roseburia inulinivorans	M D N N Y Y N N N N N N N T N S N S N Y N
C7	E7GXS5*	Streptococcus anginosus	R S G N Y V F L A N S T N R Y Q G N Y Y N
C8	F0HUU2	Lactobacillus delbrueckii	S Y S S S A N N Y G Y G S N Y N Y S Y S A
C9	F5LFB6	Paenibacillus	G Y V Q S S Y G Q N Q F Q N S Q Y G S Y Q
C10	G9Y7N7	Hafnia alvei	S T G Y S D L N S T Y N Q S A L I N Q I G

Table 1. Set of Exogenous Prion-like Sequences. *Columns (from left to right) display: sequence Identifiers used in this study; UniProt accession codes; source species from which the sequences originate; amino acid sequences, with residues colored according to the Zappo color scheme, aliphatic/hydrophobic (ILVAM) - rose, aromatic (FWY) - orange, positive (KRH) - dark blue, negative (DE) - red, hydrophilic (STNQ) - light green, conformationally special (PG) - magenta, cysteine (C) - yellow. Sequences obtained from Seira Curto et al.*[40]*.*

Our collection includes 10 sequences, each consisting of 21 amino acids with prion-like properties[40], found in different bacterial genomes and predominantly present in extracellular proteins. These sequences display compositional similarities below 30% (KAlign, UGENE, see Methods) and possess net charges between +2 and -2 (Table 1). Since these proteins originate from gut microbiome bacteria, they might reach the gut lumen either through active export or after cell lysis due to digestive activity[41,42] (Figure 1A). Once released, these sequences could interact with host cells and proteins. Based on this premise and our previous experience, we used this collection as a model to study how exogenous molecules affect the interplay between Aβ40 and Aβ42, focusing on the interference with heterotypic interactions and cross-seeding events (Figure 1C).

To mimic the complex aggregation processes observed in living organisms, we designed an approach based on sequential heterotypic seeding assays (Figures 1A and 1C). In this study, we incorporate the interplay between Aβ42 and Aβ40, hypothesizing that the higher abundance of Aβ40[5,7] facilitates encounters with exogenous molecules, thereby indirectly affecting Aβ42 aggregation and disease progression. To explore these interactions, we monitored Thioflavin-T (Th-T) fluorescence (Figures 2-4) and collected transmission electron microscopy (TEM) images (Supplementary Figures 1 and 2) to assess how Aβ42 aggregation is influenced by pre-aggregated samples assembled under different heterotypic interactions. Through these assays, we aim to shed light on the possible scenarios Aβ42 might encounter as it moves through the body (Figure 1A) and elucidate how the "Interaction History" could impact its aggregation and propagation (Figure 1C).

In our previous study[40], we found that most of the bacterial prion-like sequences (8 out of 10) speed up Aβ40 aggregation, and that the lag time correlated with the sequences' net charge. Hence, positively charged sequences led to faster aggregation, while negatively charged ones had little effect or even slowed aggregation. These results highlight the role of electrostatic forces in intermolecular interactions and align with earlier reports showing that negatively charged peptides inhibit Aβ aggregation[46,47]. In the present study, we extended our analysis to Aβ42 by incubating it with these pre-aggregated bacterial peptides. Similar to the effects observed with Aβ40, incubation of Aβ42 with a 10% molar ratio of prion-like sequences predominantly enhances its aggregation (seven samples presented shorter half-time, Figure 2).

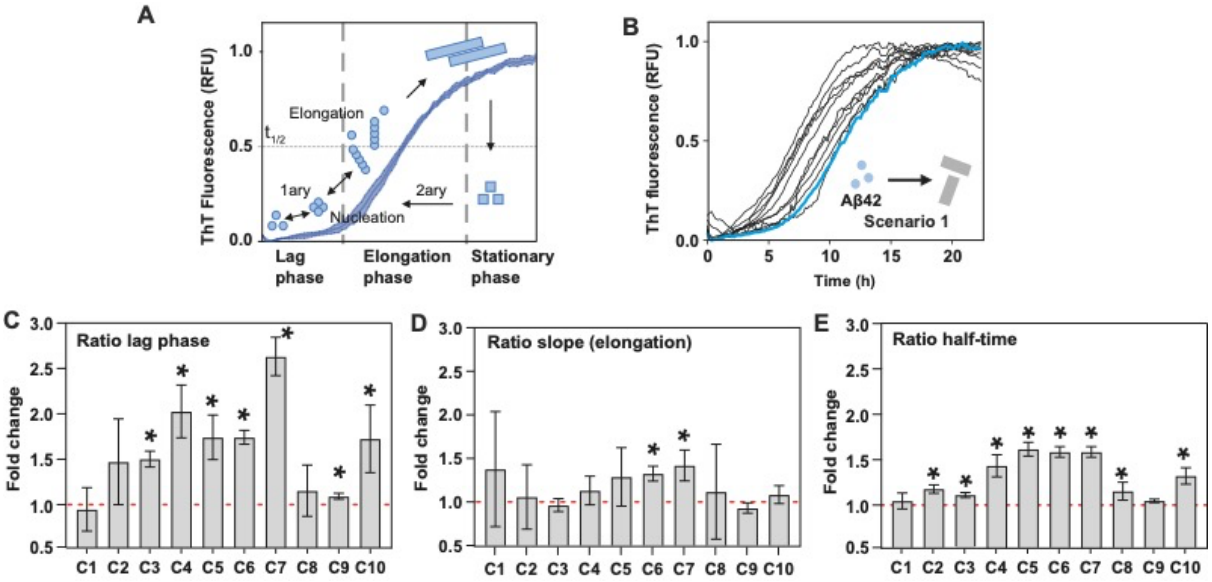

Figure 2. Exogenous Prion-like Sequences Influence Aβ42 Aggregation. *A) Aggregation kinetics of Aβ42 in the presence (C1–C10, black lines) and absence (w/o, blue line) of seeds from exogenous prion-like sequences. B) Lag phase times for Aβ42 aggregation under the same conditions as in panel A. C) Slope measurements for Aβ42 aggregation under the same conditions as in panel A. D) Half-times for Aβ42 aggregation under the same conditions as in panel A. The Y axis represents the fold change in aggregation parameters between seeded and unseeded assays (seeded/unseeded) (see Supplementary Material Figure 3). The red dashed line serves as a visual reference indicating 1.25 fold change relative to the assay containing*

only Aβ42 monomers (unseeded). An asterisk (*) indicates a statistically significant difference ($p < 0.05$) compared to the condition without seeds, as determined by an unpaired t-test. Error bars indicate the standard deviation. Each condition represents the results of three biological replicates, with three technical replicates per biological replicate.

Although no clear correlation with net charge was observed, it is noteworthy that the peptides most strongly accelerating Aβ40 aggregation (C7 and C4)[40] also resulted in shorter lag times in Aβ42 aggregation kinetics (Figure 2C). In general, the observed enhancement in the aggregation curves appears to be primarily attributed to a shorter lag phase, as only two samples exhibited steeper slopes, while seven displayed shortened lag times (Figure 2B-D). A reduced lag time indicates a more efficient primary nucleation phase, involving oligomeric species that serve as templates, whereas a steeper slope indicates a faster aggregation rate during the growth phase, which can include the rapid addition of monomers to existing fibrils and more secondary nucleation events (Figure 2A). The half-time (t1/2) serves as an indicator of overall aggregation efficiency, influenced by both lag phase and slope. Together, these findings suggest that these exogenous prion-like sequences primarily enhance the nucleation of Aβ42 aggregation by acting as seeding points (Figure 2).

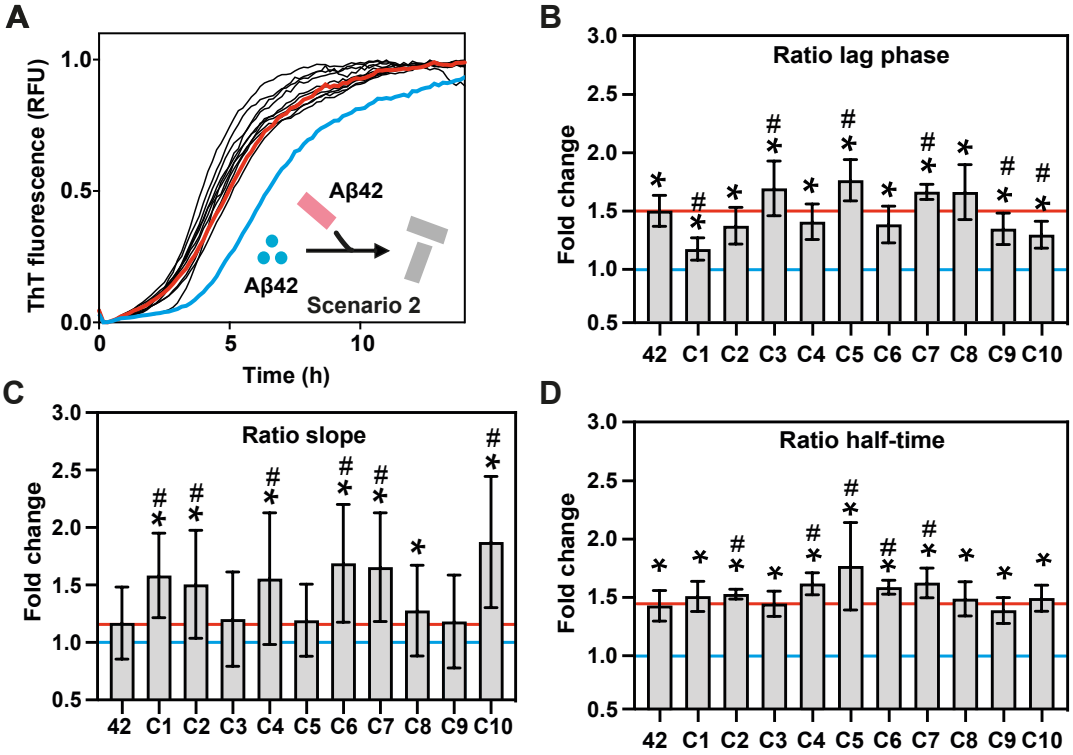

Figure 3. Exogenous Prion-like Sequences Affect Aβ42 Seeds and Their Propagation. *A) Aggregation kinetics of Aβ42 seeded with Aβ42 aggregates formed in the presence (C1–C10) and absence (w/o) of seeds from exogenous prion-like sequences. B) Lag phase times for Aβ42 aggregation under the same conditions as in panel A. C) Slope measurements for Aβ42 aggregation under the same conditions as in panel A. D) Half-times for Aβ42 aggregation under the same conditions as in panel A. The Y axis represents the fold change in aggregation parameters between seeded and unseeded assays (seeded/unseeded) (see Supplementary Material Figure 4). An asterisk (*) indicates a statistically significant difference ($p < 0.05$) compared to the condition without seeds, as determined by an unpaired t-test. A hash symbol (#) indicates a statistically significant difference ($p < 0.05$) compared to the condition seeded*

with pure Aβ42 aggregates, determined by an unpaired t-test. Blue Line and "w/o" column represent the aggregation kinetics of Aβ42 without any seeds. Red Line and "42" column represent the aggregation kinetics of Aβ42 seeded with pure Aβ42 aggregates. Error bars indicate the standard deviation. Each condition represents the results of three biological replicates, with three technical replicates per biological replicate.

Effect on Aβ42 Seeds and Their Propagation

After observing that bacterial prion-like sequences influence the aggregation of both Aβ40 and Aβ42, we investigated how past molecular interactions (here referred to as "Interaction History") affect the propagation of Aβ42 aggregates (Figure 1C). To address this, we conducted kinetic assays using pre-formed Aβ fibrils previously seeded with the bacterial peptides (Figure 2, Supplementary Figure 3). This second aggregation step (Figure 1C; Figure 3) involved a tenfold dilution of the exogenous peptides compared to the initial direct seeding assays. This dilution was achieved by incorporating 10% of the Aβ aggregates formed during the first step (Methods), keeping minimal the influence from the bacterial molecules and allowing us to focus on the properties of the pre-formed aggregates.

All lag times were accelerated compared to Aβ42 without seeds, with three bacterial sequences even outperforming the kinetics seeded with pure Aβ42 aggregates, which were formed just by Aβ42 molecules (Figure 3B, # symbol). Regarding the slope, seven sequences exhibited faster elongation/secondary nucleation effects compared to unseeded monomers, while six out of ten presented significantly steeper slopes than those triggered by the pure Aβ42 seeds. These findings point to an amplification effect, where the presence of bacterial peptides modifies the Aβ42 aggregated material, enhancing its seeding capabilities. This also underscores the importance of the Interaction History, demonstrating that even exogenous molecules with limited initial seeding capability can produce aggregates with enhanced subsequent aggregation potential. Overall, while the first-step assay using only bacterial sequences as seeds predominantly affected the primary nucleation phase, this subsequent aggregation assay shows that Aβ42 aggregates are also efficient in recruiting monomers and promoting secondary nucleation events, further supporting the concept that sequence similarity favors the cross-seeding efficiency [48].

Beyond the overall acceleration of aggregation kinetics, our analysis of the Aβ42 seeds revealed that incubation with bacterial prion-like sequences (Figure 3A-D, Supplementary Figure 4) produces aggregates with varied seeding effects. Specifically, some bacterial peptides (C7) reduce both lag time and slope, while others selectively affect one parameter (C1, C2, C3, C4, C5, C6, C10), and some have no significant effects (C8) or even delay the aggregation process (C9).

These results indicate that exogenous molecules can interfere with different phases of host protein aggregation, affecting subsequent interactions and influencing aggregate propagation, even in the absence of exogenous peptides during later stages. For instance, peptide C5 appears to enhance monomer adherence during the initial nucleation phase, while peptide C4 seems to accelerate elongation by promoting secondary nucleation. This diversity in mechanism modulating Aβ42 aggregation may increase the structural heterogeneity of amyloid fibrils, further complicating the pathological landscape of Alzheimer's disease.

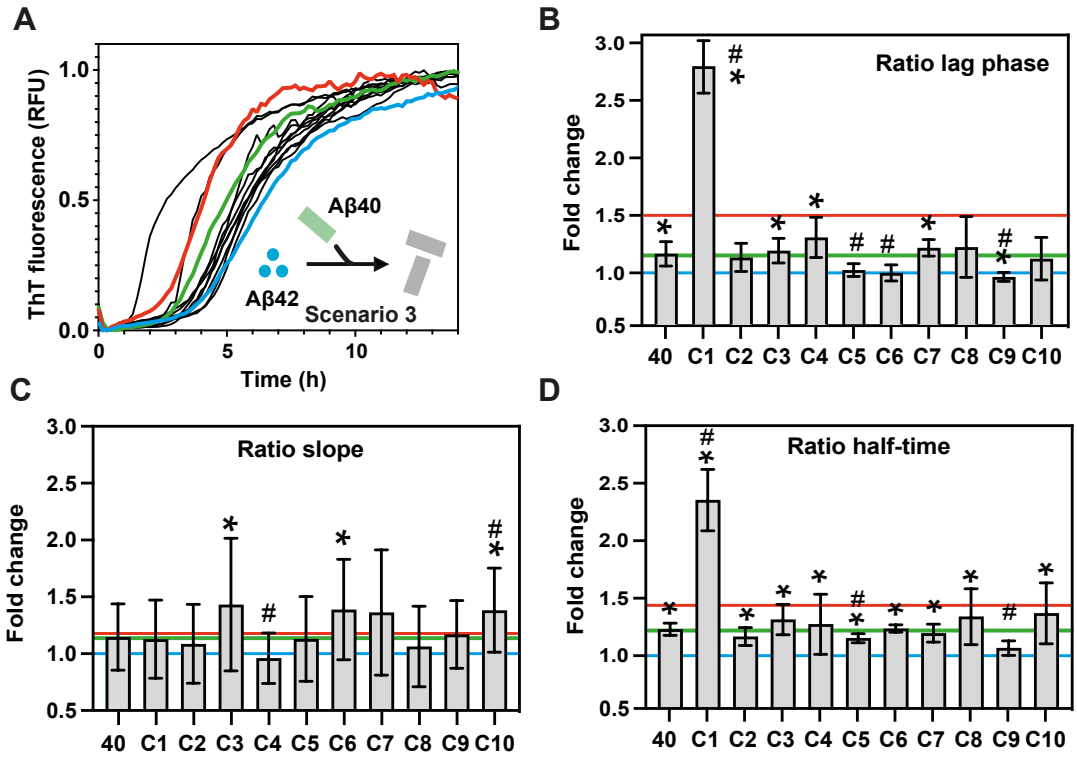

Figure 4. Exogenous Prion-like Sequences Affect Aβ40 Aggregation and Its Propagation to Aβ42. *A) Aggregation kinetics of Aβ42 seeded with Aβ40 aggregates formed in the presence (C1–C10) and absence (w/o) of seeds from exogenous prion-like sequences. B) Lag phase times for Aβ42 aggregation under the same conditions as in panel A. C) Slope measurements for Aβ42 aggregation under the same conditions as in panel A. D) Half-times for Aβ42 aggregation under the same conditions as in panel A. The Y axis represents the fold change in aggregation parameters between seeded and unseeded assays (seeded/unseeded) (see Supplementary Material Figure 5). An asterisk (*) indicates a statistically significant difference ($p < 0.05$) compared to the condition without seeds, as determined by unpaired t-test. A hash symbol (#) indicates a statistically significant difference ($p < 0.05$) compared to the condition seeded with pure Aβ40 aggregate, determined by an unpaired t-test. Blue Line represents the aggregation kinetics of Aβ42 without any seeds. Red Line represents the aggregation kinetics of Aβ42 seeded with pure Aβ42 aggregates. Green Line and "40" column represent the aggregation kinetics of Aβ42 seeded with pure Aβ40 aggregates. Error bars indicate the standard deviation. Each condition represents the results of three biological replicates, with three technical replicates per biological replicate.*

Effect on Aβ40 and Its Subsequent Seeding of Aβ42

While the previous experiments focused on the self-seeding of Aβ42, it is important to consider that Aβ40 is the predominant isoform of amyloid-beta peptide in the human body[5,7]. Given its higher abundance, Aβ40 is more likely to encounter and interact with exogenous prion-like proteins. To explore this possibility, we examined whether our collection of exogenous sequences could also influence the cross-seeding potential of Aβ40 on Aβ42 (Figure 4, Supplementary Figure 5).

In previous studies, we observed that most bacterial sequences, from our collection, accelerated the aggregation of monomeric Aβ40[40]. In the present study, we used Aβ40

aggregates formed during this initial aggregation step to seed Aβ42 deposition. As a control, we tested the seeding efficiency of pure Aβ40 aggregates (assembled solely from Aβ40 molecules) and found that, although they reduced the lag time and half-time of Aβ42 aggregation to a lesser extent than Aβ42 seeds, they induced a comparable slope increase. These findings suggest that residues 41 and 42 play a critical role in facilitating the assembly of free monomers during the primary nucleation process, and their absence in Aβ40 reduces its propagation efficiency[49].

When analyzing the effects of Aβ40 aggregates formed in the presence of the bacterial peptides, we observed that only four of the ten shortened the lag phase, and among these, only one (C1) achieved a lag time shorter than that of pure Aβ40 aggregates. Interestingly, three of these peptides also steepened the slope, showing that incubation with bacterial molecules can produce aggregates capable of influencing distinct aggregation phases. Overall, seven out of ten peptides significantly reduced the half-time of Aβ42 aggregation. However, only C1 achieved a half-life shorter than that of pure Aβ40 and, more notably, also shorter than pure Aβ42 aggregates (red line, p-value < 0.05, unpaired t-test). In contrast, some bacterial peptides, such as C5 and C9, slowed this subsequent aggregation process (Figure 4, Supplementary Figure 5).

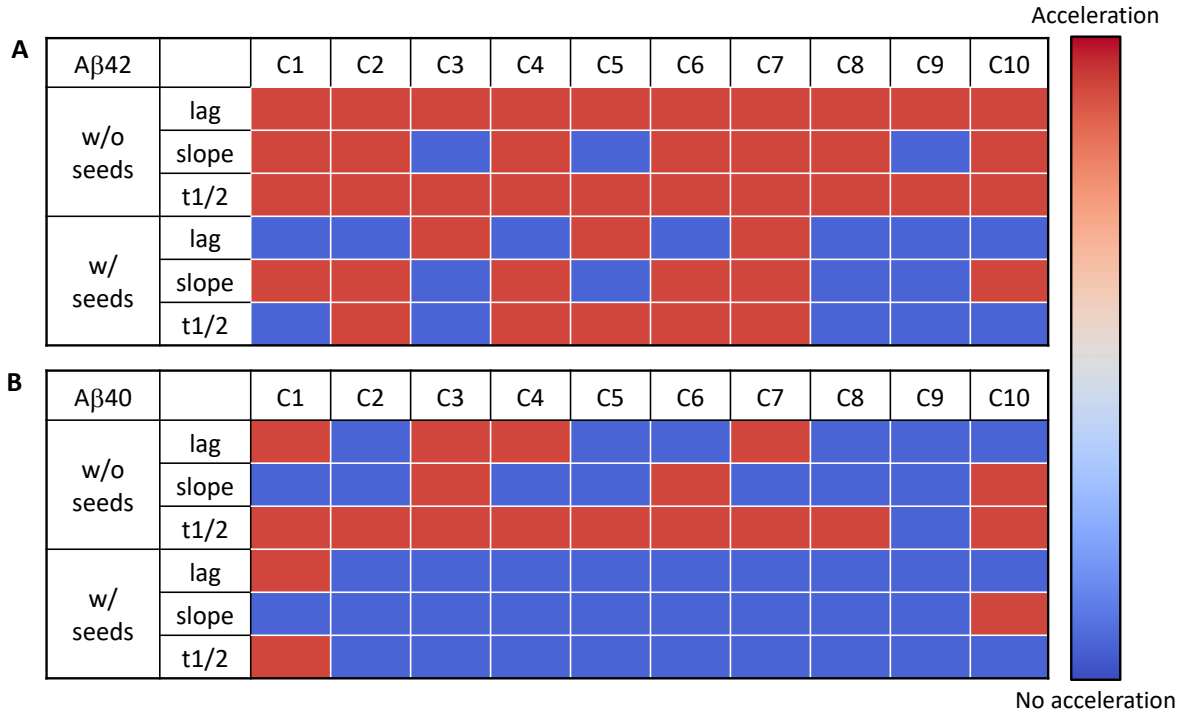

Figure 5. Differential Effects of Exogenous Prion-like Sequences on Aβ42 Aggregation*. This figure provides a schematic overview of the significance data presented in Figure 3 and 4. It presents two heatmaps illustrating the impact of exogenous prion-like sequences on Aβ42 aggregation, when it is a posterior or a second-step process. Red indicates conditions that significantly accelerate Aβ42 aggregation, while blue indicates conditions with no significant acceleration. In the second column, t1/2 represents comparisons of half-times, and lag represents comparisons of lag phase durations. w/o seeds refer to comparisons with the aggregation kinetics of Aβ42 without any added seeds, and w/ seeds refer to comparisons made with Aβ42 seeded with pure Aβ42 aggregates. A) Heat map summarizing results from assays using Aβ42 aggregates as seeds. B) Heat map summarizing results from assays using*

Aβ40 aggregates as seeds. The first row of each heatmap shows the names of the specific exogenous sequences added during the formation of the seeds.

The limited effect of bacterial peptides on Aβ40 aggregation (Figure 5) raises intriguing questions about potential evolutionary adaptations of Aβ40 that may reduce harmful interactions with exogenous molecules[50,51]. These findings suggest that Aβ40 is more resilient to external amyloid sequences, making it less likely to propagate an aggregative conformation throughout the organism. Interestingly, C1, the only sequence able to break this resilience, originates from a putative vacuolating cytotoxin of *Helicobacter pylori*, a bacterium associated with Alzheimer's disease[52,53]. Consistent with this, our previous work[40] demonstrated that the C1 sequence favored yeast Sup35 prion propagation and caused one of the most pronounced negative effects on *C. elegans* cognitive abilities.

These findings highlight the potential for exogenous amyloid sequences to modulate not only direct seeding processes but also posterior cross-seeding events between different Aβ isoforms. The impact on the seeding potential varies among exogenous molecules, suggesting that specific molecular properties determine the extent and direction of their influence. Furthermore, the ability of certain sequences to either enhance or inhibit the aggregation propagation may inspire the development of novel therapeutic strategies.

Our data also suggest that exogenous amyloids may expand the structural diversity of the protein aggregates in the brain. Previous studies have identified multiple fibril polymorphs derived from patient brain samples, revealing structural heterogeneity among amyloid deposits[22,38,54]. The introduction of exogenous prion-like sequences could further contribute to this polymorphism, complicating the pathological landscape of Alzheimer's disease.

Conclusions

Our study demonstrates that exogenous amyloid sequences can significantly influence Aβ aggregation dynamics through a mechanism we term Interaction History. These sequences can seed alternative aggregation structures of $A\beta_{42}$, which may impact both the toxicity and structural properties of the resulting fibrils. This highlights the potential role of environmental factors, particularly amyloids from gut microbiota, in modulating Aβ aggregation and subsequent neurodegeneration[40] **.**

The observed diversity in aggregate characteristics underscores the complexity of Aβ pathology [22,38,54], suggesting that therapeutic strategies should address a broad spectrum of amyloid configurations to effectively mitigate neurodegenerative processes. Our findings indicate that the gut microbiome[33,34,39], especially amyloid-producing microbes like *H. pylori* [52,53], may play an unappreciated role in influencing Aβ aggregation within the brain. This opens new avenues for understanding the intricate interactions between environmental factors and Alzheimer's disease pathology.

The results presented here underscore the importance of Interaction History, demonstrating that molecules with limited initial seeding capability can generate assemblies capable of efficiently triggering secondary aggregation events. This evidence has multiple implications. First, heterologous assemblies may produce an amplification effect that can exacerbate disease progression. Second, these findings indicate that the absence of seeding effect in a

single-step aggregation assay may be misleading without validating the results through subsequent aggregation assays. Furthermore, since an exogenous molecule can influence subsequent interactions, the propagation of aggregates can occur far from the original site of infection and even in the absence of the exogenous molecule, making it difficult to identify the responsible agent.

Understanding protein aggregation in the presence of exogenous molecules can provide valuable insights into disease mechanisms. Moreover, these findings underscore the need to consider environmental and microbial influences in developing effective therapeutic strategies for Alzheimer's disease and related conditions.

Methods

Protein alignment and consensus sequence

The alignments between the 10 different amyloid-forming core candidates and the consensus sequence were obtained using the KAling method within the Unipro UGENE software v43.0 [55]. Unipro UGENE software v43.0 was also used for sequence representation.

Peptide Preparation

All samples were prepared in low protein-binding microcentrifuge tubes (ThermoFisher Scientific, Waltham, MA, USA). The bacterial amyloid sequences were obtained in lyophilized form from the Peptide Synthesis Facility, Department of Experimental and Health Sciences, Universitat Pompeu Fabra (UPF). Peptides were initially solubilized in 1,1,1,3,3,3-hexafluoroisopropanol (HFIP), then divided into aliquots and dried overnight in a fume hood at room temperature. For the amyloid aggregation, we employed the same conditions as in Curto, J.S. *et al.* 2024[40], in brief, the peptides were dissolved in DMSO to maintain monomeric states, followed by dilution in 50 mM phosphate buffer (PB), pH 7.4.

Synthetic Aβ40 and Aβ42 were purchased from GenScript (Rijswijk, Netherlands). Stock solutions were prepared by dissolving 1 mg of peptide in a final concentration of 250 µM in 20 mM sodium phosphate buffer with 0.04% NH_3 and NaOH to achieve a pH of 11. The absence of aggregates was assessed using dynamic light scattering[40,56]. The peptide solution was then sonicated for 10 minutes (Fisherbrand Pittsburgh, PA, USA, FB15051) without sweep mode and stored at −80°C. For seeding experiments, the peptide was diluted at a 20 uM concentration 50 mM phosphate buffer (PB), pH 7.4. Then, if necessary, the specific seeds were added to a final concentration of 2 uM and the mixture was left to aggregate at room temperature for 24 hours before their analysis.

Thioflavin-T Binding and Aggregation Kinetics

Thioflavin-T (ThT) was dissolved in Milli-Q water to a concentration of 5 mM, filtered through a 0.2-µm filter, diluted to 0.5 mM, and stored at −20°C. ThT fluorescence for aggregation kinetics was measured every 10 minutes, and endpoint readings for ThT binding were obtained using a 440-nm excitation filter and a 480-nm emission filter on a plate reader (TECAN Infinite+ NANO) with bottom optics. Samples were prepared in flat-bottom, black, non-binding 96-well plates (Greiner Bio-One), with 100 µL of sample added per well. Each condition was measured in triplicate.

For seeding experiments, Aβ40 and Aβ42 peptide stocks at pH 11 were diluted to a final concentration of 25 µM in 20 mM sodium phosphate buffer with 100 mM NaCl. The corresponding pre-aggregated peptides were sonicated for 5 minutes before being added to a final concentration of 2.5 µM. Control conditions included samples without Aβ40 but with the peptide, samples without Aβ42, and samples without peptides, all prepared with equivalent volumes of the corresponding buffers. All samples and controls were prepared in triplicate. The pH in each well was measured at the beginning and end of the experiment to confirm stability throughout the aggregation process and to verify consistency across conditions. ThT was added to a final concentration of 20 µM. Aggregation reactions were conducted at 37°C without agitation, with four independent replicates. The $t_{1/2}$, defined as the time to reach 50% of the final fluorescence intensity, was recorded for each condition. The lag phase was calculated as the time to reach 10% of the final fluorescence intensity. Each condition was measured with three experimental replicates, each consisting of three technical replicates. Also, the data were fitted into a sigmoidal curve using the Hill function

$$h(x) = A\frac{x^h}{x^h + K^h}$$

Being A, h and K the fitting parameters. The fittings were used to calculate the slope of the exponential phase of the aggregation kinetic as done by Rupert et al[23].

Transmission Electron Microscopy (TEM)

To prepare samples for TEM analysis, a 10 µL aliquot of the aggregated peptide solution (25 µM, incubated at 37°C for 24 hours without agitation) was applied to carbon-coated copper grids and allowed to adhere for 1 minute. Liquid excess was carefully blotted with Whatman filter paper[40]. Grids were then rinsed with distilled water and subsequently stained with 2% (w/v) uranyl acetate for 1 minute. After staining, grids were air-dried. Micrographs were obtained using a JEM-1400 transmission electron microscope (JEOL, Tokyo, Japan) set to an accelerating voltage of 80 keV.

Funding

This work was funded by grants RYC2019-026752-I, CNS2023-144437/MCIN/AEI/10.13039/501100011033, PID2020-117454RA-I00/AEI/10.13039/501100011033 from Ministerio de Ciencia e Innovación and by L'Oréal-UNESCO For Women in Science Programme.

Acknowledgments

We extend our gratitude to the following individuals:

Nuria Benseny for her assistance in the microFTIR experiments.

Josep Cladera for his responses and discussions around the investigation.

µFTIR experiments were performed at MIRAS beamline at ALBA Synchrotron with the collaboration of ALBA staff.

Transmission electron microscopy (TEM) images were acquired at the Servei de Microscòpia i Difracció de Raigs X (SMiDRX) of the Universitat Autònoma de Barcelona (UAB).

Bibliography

1. Holmes, B. B. & Diamond, M. I. Cellular mechanisms of protein aggregate propagation. *Curr. Opin. Neurol.* **25**, 721–726 (2012).
2. Hebert, L. E., Scherr, P. A., Bienias, J. L., Bennett, D. A. & Evans, D. A. Alzheimer disease in the US population: prevalence estimates using the 2000 census. *Arch. Neurol.* **60**, 1119–1122 (2003).
3. Chiti, F. & Dobson, C. M. Protein Misfolding, Amyloid Formation, and Human Disease: A Summary of Progress Over the Last Decade. *Annu. Rev. Biochem.* **86**, 27–68 (2017).
4. Chiti, F. & Dobson, C. M. Protein misfolding, functional amyloid, and human disease. *Annu. Rev. Biochem.* **75**, 333–366 (2006).
5. Guo, T. *et al.* Molecular and cellular mechanisms underlying the pathogenesis of Alzheimer's disease. *Mol. Neurodegener.* **15**, (2020).
6. Hampel, H. *et al.* The Amyloid-β Pathway in Alzheimer's Disease. *Mol. Psychiatry* **26**, 5481–5503 (2021).
7. Chen, G. F. *et al.* Amyloid beta: structure, biology and structure-based therapeutic development. *Acta Pharmacol. Sin.* **38**, 1205–1235 (2017).
8. Sulatskaya, A. I. *et al.* New Evidence on a Distinction between Aβ40 and Aβ42 Amyloids: Thioflavin T Binding Modes, Clustering Tendency, Degradation Resistance, and Cross-Seeding. *Int. J. Mol. Sci.* **23**, (2022).
9. Tran, J., Chang, D., Hsu, F., Wang, H. & Guo, Z. Cross-seeding between Aβ40 and Aβ42 in Alzheimer's disease. *FEBS Lett.* **591**, 177–185 (2017).
10. Gu, L. & Guo, Z. Alzheimer's Aβ42 and Aβ40 peptides form interlaced amyloid fibrils. *J. Neurochem.* **126**, 305–311 (2013).
11. Yang, Y. *et al.* Cryo-EM structures of amyloid-β 42 filaments from human brains. *Science* **375**, 167–172 (2022).
12. Braun, G. A., Dear, A. J., Sanagavarapu, K., Zetterberg, H. & Linse, S. Amyloid-β peptide 37, 38 and 40 individually and cooperatively inhibit amyloid-β 42 aggregation. *Chem. Sci.* **13**, 2423–2439 (2022).
13. Suire, C. N. *et al.* Cathepsin D regulates cerebral Aβ42/40 ratios via differential degradation of Aβ42 and Aβ40. *Alzheimers. Res. Ther.* **12**, (2020).
14. Kwak, S. S. *et al.* Amyloid-β42/40 ratio drives tau pathology in 3D human neural cell culture models of Alzheimer's disease. *Nat. Commun.* **11**, (2020).
15. Liu, C. C. *et al.* ApoE4 Accelerates Early Seeding of Amyloid Pathology. *Neuron* **96**, 1024-1032.e3 (2017).
16. Lee, M., Yau, W. M., Louis, J. M. & Tycko, R. Structures of brain-derived 42-residue amyloid-β fibril polymorphs with unusual molecular conformations and intermolecular interactions. *Proc. Natl. Acad. Sci. U. S. A.* **120**, (2023).
17. Xiong, F., Ge, W. & Ma, C. Quantitative proteomics reveals distinct composition of amyloid plaques in Alzheimer's disease. *Alzheimers. Dement.* **15**, 429–440 (2019).
18. Rahman, M. M. & Lendel, C. Extracellular protein components of amyloid plaques and their roles in Alzheimer's disease pathology. *Mol. Neurodegener.* **16**, (2021).
19. Bharadwaj, P. *et al.* Amylin and beta amyloid proteins interact to form amorphous heterocomplexes with enhanced toxicity in neuronal cells. *Sci. Rep.* **10**, (2020).
20. Shim, K. H., Kang, M. J., Youn, Y. C., An, S. S. A. & Kim, S. Y. Alpha-synuclein: a pathological factor with Aβ and tau and biomarker in Alzheimer's disease. *Alzheimers. Res. Ther.* **14**, (2022).

21. Clinton, L. K., Blurton-Jones, M., Myczek, K., Trojanowski, J. Q. & LaFerla, F. M. Synergistic Interactions between Abeta, tau, and alpha-synuclein: acceleration of neuropathology and cognitive decline. *J. Neurosci.* **30**, 7281–7289 (2010).
22. Ivanova, M. I., Lin, Y., Lee, Y. H., Zheng, J. & Ramamoorthy, A. Biophysical processes underlying cross-seeding in amyloid aggregation and implications in amyloid pathology. *Biophys. Chem.* **269**, (2021).
23. Rupert, J., Monti, M., Zacco, E. & Tartaglia, G. G. RNA sequestration driven by amyloid formation: the alpha synuclein case. *Nucleic Acids Res.* **51**, 11466–11478 (2023).
24. Janas, T., Sapoń, K., Stowell, M. H. B. & Janas, T. Selection of Membrane RNA Aptamers to Amyloid Beta Peptide: Implications for Exosome-Based Antioxidant Strategies. *Int. J. Mol. Sci.* **20**, (2019).
25. Álvarez-Marimon, E. *et al.* Synchrotron X-ray Fluorescence and FTIR Signatures for Amyloid Fibrillary and Nonfibrillary Plaques. *ACS Chem. Neurosci.* **12**, 1961–1971 (2021).
26. Abelein, A. Metal Binding of Alzheimer's Amyloid-β and Its Effect on Peptide Self-Assembly. *Acc. Chem. Res.* **56**, 2653–2663 (2023).
27. Pithadia, A. S. & Lim, M. H. Metal-associated amyloid-β species in Alzheimer's disease. *Curr. Opin. Chem. Biol.* **16**, 67–73 (2012).
28. Tittelmeier, J., Druffel-Augustin, S., Alik, A., Melki, R. & Nussbaum-Krammer, C. Dissecting aggregation and seeding dynamics of α-Syn polymorphs using the phasor approach to FLIM. *Commun. Biol.* **5**, (2022).
29. Seira Curto, J., Fernandez, M. R., Cladera, J., Benseny-Cases, N. & Sanchez de Groot, N. Aβ40 Aggregation under Changeable Conditions. *Int. J. Mol. Sci.* **24**, (2023).
30. Tycko, R. Amyloid polymorphism: structural basis and neurobiological relevance. *Neuron* **86**, 632–645 (2015).
31. Duran-Aniotz, C. *et al.* Amyloid pathology arrangements in Alzheimer's disease brains modulate in vivo seeding capability. *Acta Neuropathol. Commun.* **9**, (2021).
32. Zhang, J. *et al.* Recent advances in Alzheimer's disease: Mechanisms, clinical trials and new drug development strategies. *Signal Transduct. Target. Ther.* **9**, (2024).
33. Belkaid, Y. & Hand, T. W. Role of the microbiota in immunity and inflammation. *Cell* **157**, 121–141 (2014).
34. Seira Curto, J. *et al.* Microbiome Impact on Amyloidogenesis. *Front. Mol. Biosci.* **9**, (2022).
35. Ren, B. *et al.* Fundamentals of cross-seeding of amyloid proteins: an introduction. *J. Mater. Chem. B* **7**, 7267–7282 (2019).
36. Sigurdson, C. J. *et al.* A molecular switch controls interspecies prion disease transmission in mice. *J. Clin. Invest.* **120**, 2590–2599 (2010).
37. Weissmann, C., Enari, M., Klöhn, P. C., Rossi, D. & Flechsig, E. Transmission of prions. *J. Infect. Dis.* **186 Suppl 2**, (2002).
38. Chaudhuri, P., Prajapati, K. P., Anand, B. G., Dubey, K. & Kar, K. Amyloid cross-seeding raises new dimensions to understanding of amyloidogenesis mechanism. *Ageing Res. Rev.* **56**, (2019).
39. Oliphant, K. & Allen-Vercoe, E. Macronutrient metabolism by the human gut microbiome: major fermentation by-products and their impact on host health. *Microbiome* **7**, (2019).
40. Curto, J. S. *et al.* Microbiome-Derived Prion-Like Proteins and Their Potential to Trigger Cognitive Dysfunction. *bioRxiv* 2023.10.19.563052 (2024)

doi:10.1101/2023.10.19.563052.
41. Holmqvist, S. *et al.* Direct evidence of Parkinson pathology spread from the gastrointestinal tract to the brain in rats. *Acta Neuropathol.* **128**, 805–820 (2014).
42. Kim, S. K. *et al.* Role of Probiotics in Human Gut Microbiome-Associated Diseases. *J. Microbiol. Biotechnol.* **29**, 1335–1340 (2019).
43. Sabate, R., Rousseau, F., Schymkowitz, J. & Ventura, S. What makes a protein sequence a prion? *PLoS Comput. Biol.* **11**, (2015).
44. Pallarès, I., Iglesias, V. & Ventura, S. The Rho Termination Factor of Clostridium botulinum Contains a Prion-Like Domain with a Highly Amyloidogenic Core. *Front. Microbiol.* **6**, (2016).
45. Esteras-Chopo, A., Serrano, L. & López De La Paz, M. The amyloid stretch hypothesis: recruiting proteins toward the dark side. *Proc. Natl. Acad. Sci. U. S. A.* **102**, 16672–16677 (2005).
46. Liao, Y. H., Chang, Y. J., Yoshiike, Y., Chang, Y. C. & Chen, Y. R. Negatively charged gold nanoparticles inhibit Alzheimer's amyloid-β fibrillization, induce fibril dissociation, and mitigate neurotoxicity. *Small* **8**, 3631–3639 (2012).
47. Chan, H. M. *et al.* Effect of surface-functionalized nanoparticles on the elongation phase of beta-amyloid (1-40) fibrillogenesis. *Biomaterials* **33**, 4443–4450 (2012).
48. Krebs, M. R. H., Morozova-Roche, L. A., Daniel, K., Robinson, C. V. & Dobson, C. M. Observation of sequence specificity in the seeding of protein amyloid fibrils. *Protein Sci.* **13**, 1933–1938 (2004).
49. Meisl, G. *et al.* Differences in nucleation behavior underlie the contrasting aggregation kinetics of the Aβ40 and Aβ42 peptides. *Proc. Natl. Acad. Sci. U. S. A.* **111**, 9384–9389 (2014).
50. Jan, A. *et al.* Abeta42 neurotoxicity is mediated by ongoing nucleated polymerization process rather than by discrete Abeta42 species. *J. Biol. Chem.* **286**, 8585–8596 (2011).
51. Haass, C. & Selkoe, D. J. Soluble protein oligomers in neurodegeneration: lessons from the Alzheimer's amyloid beta-peptide. *Nat. Rev. Mol. Cell Biol.* **8**, 101–112 (2007).
52. Vogt, N. M. *et al.* Gut microbiome alterations in Alzheimer's disease. *Sci. Rep.* **7**, (2017).
53. Panza, F., Lozupone, M., Solfrizzi, V., Watling, M. & Imbimbo, B. P. Time to test antibacterial therapy in Alzheimer's disease. *Brain* **142**, 2905–2929 (2019).
54. Rasmussen, J. *et al.* Amyloid polymorphisms constitute distinct clouds of conformational variants in different etiological subtypes of Alzheimer's disease. *Proc. Natl. Acad. Sci. U. S. A.* **114**, 13018–13023 (2017).
55. Okonechnikov, K., Golosova, O., Fursov, M. & UGENE team. Unipro UGENE: a unified bioinformatics toolkit. *Bioinformatics* **28**, 1166–7 (2012).
56. Benseny-Cases, N., Klementieva, O. & Cladera, J. In vitroOligomerization and Fibrillogenesis of Amyloid-beta Peptides. *Subcell. Biochem.* **65**, 53–74 (2012).

Supplementary Material

Exogenous Amyloid Sequences: Their Role in Amyloid-Beta Heterotypic Aggregation

Jofre Seira Curto[1], Sandra Villegas Hernandez[1], Maria Rosario Fernandez[1], Natalia Sanchez de Groot[1]*
[1]Unitat de Bioquímica. Departament de Bioquímica i Biologia Molecular. Universitat Autònoma de Barcelona, Spain.

Supplementary Figure 1. TEM Images of Fibrillar Aggregates of Aβ42 Seeded with Aβ42

Supplementary Figure 2. TEM Images of Fibrillar Aggregates of Aβ42 Seeded with Aβ40.

Supplementary Figure 3. Aggregation kinetics of Aβ42 incubated with different bacterial amyloid cores.

Supplementary Figure 4. Aggregation kinetics of Aβ42 incubated with different seeds of Aβ42.

Supplementary Figure 5. Aggregation kinetics of Aβ42 incubated with different seeds of Aβ40

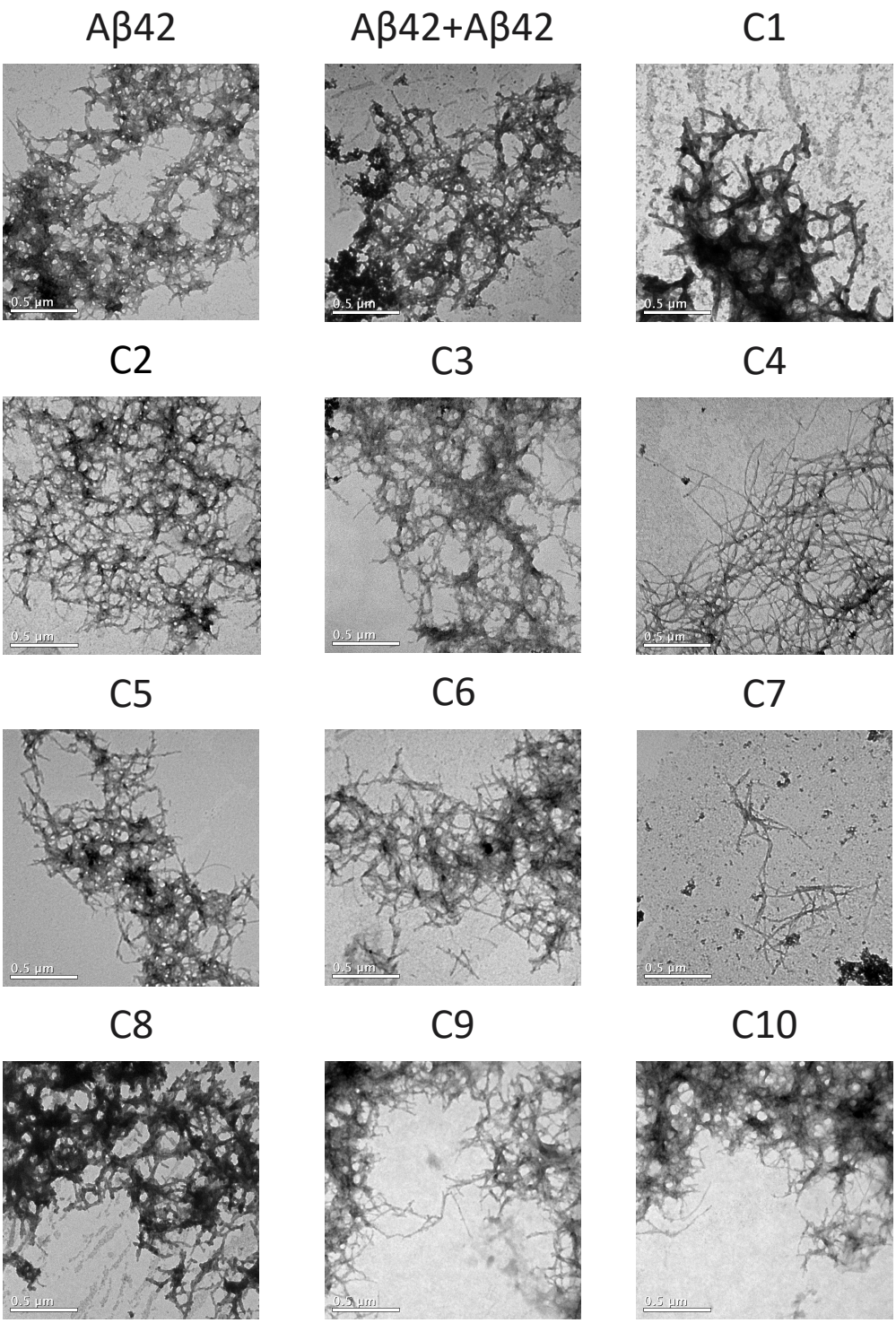

Supplementary Figure 1. TEM Images of Fibrillar Aggregates of Aβ42 Seeded with Aβ42. This figure presents transmission electron microscopy (TEM) images showing fibrillar aggregates of Aβ42 under different seeding conditions. The top left image shows Aβ42 aggregated without added seeds, while the top middle image shows Aβ42 aggregated with pure Aβ42 seeds. The remaining images illustrate Aβ42 aggregates seeded with Aβ42 fibrils formed in the presence of the indicated amyloid core sequences. All aggregates were formed after 24 hours of incubation at 37ºC without agitation.

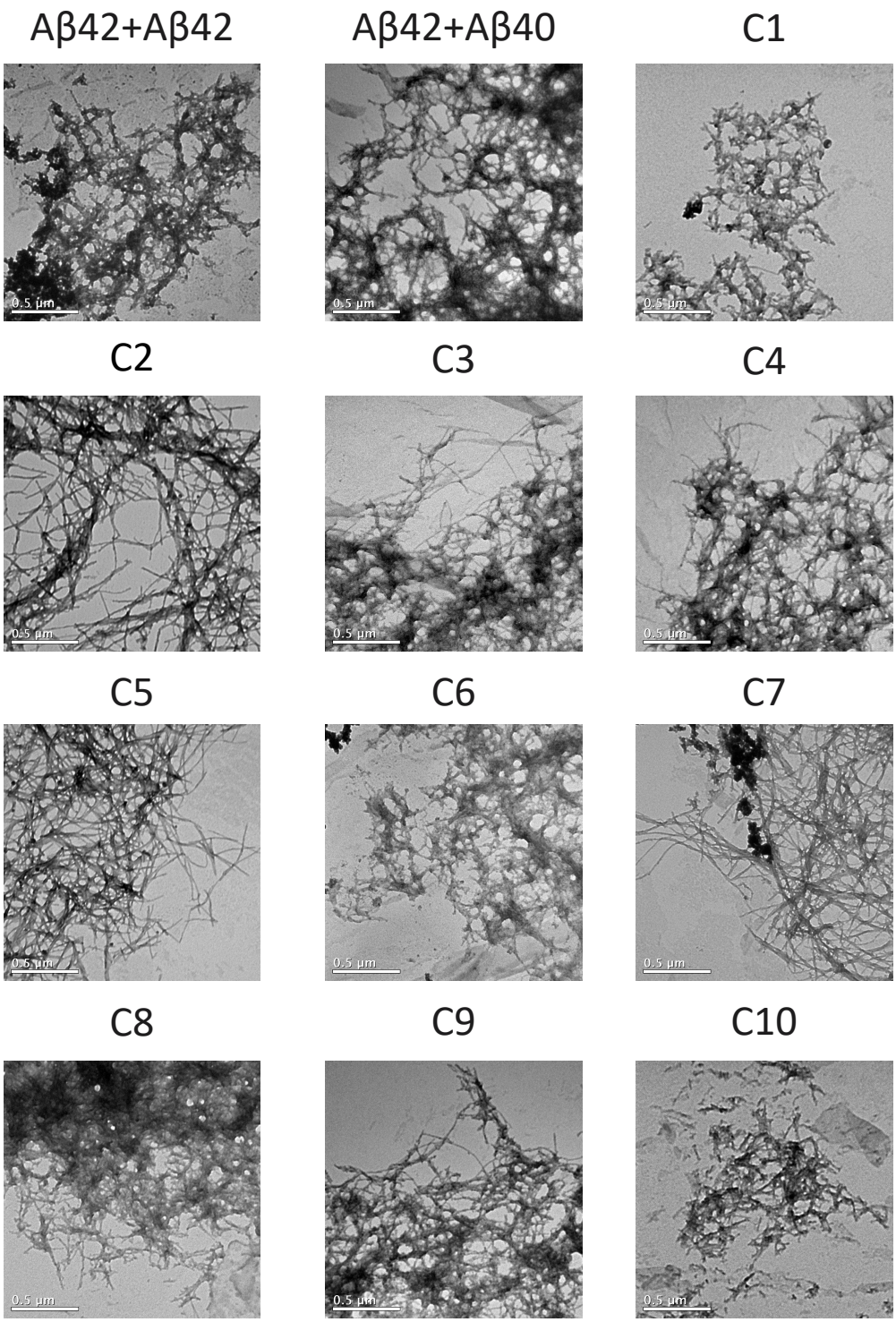

Supplementary Figure 2. TEM Images of Fibrillar Aggregates of Aβ42 Seeded with Aβ40. This figure presents transmission electron microscopy (TEM) images showing fibrillar aggregates of Aβ42 under different seeding conditions. The top left image shows Aβ42 aggregated with pure Aβ42 seeds, while the top middle image shows Aβ42 aggregated with pure Aβ40 seeds. The remaining images illustrate Aβ42 aggregates seeded with Aβ40 fibrils formed in the presence of the indicated amyloid core sequences. All aggregates were formed after 24 hours of incubation at 37ºC without agitation.

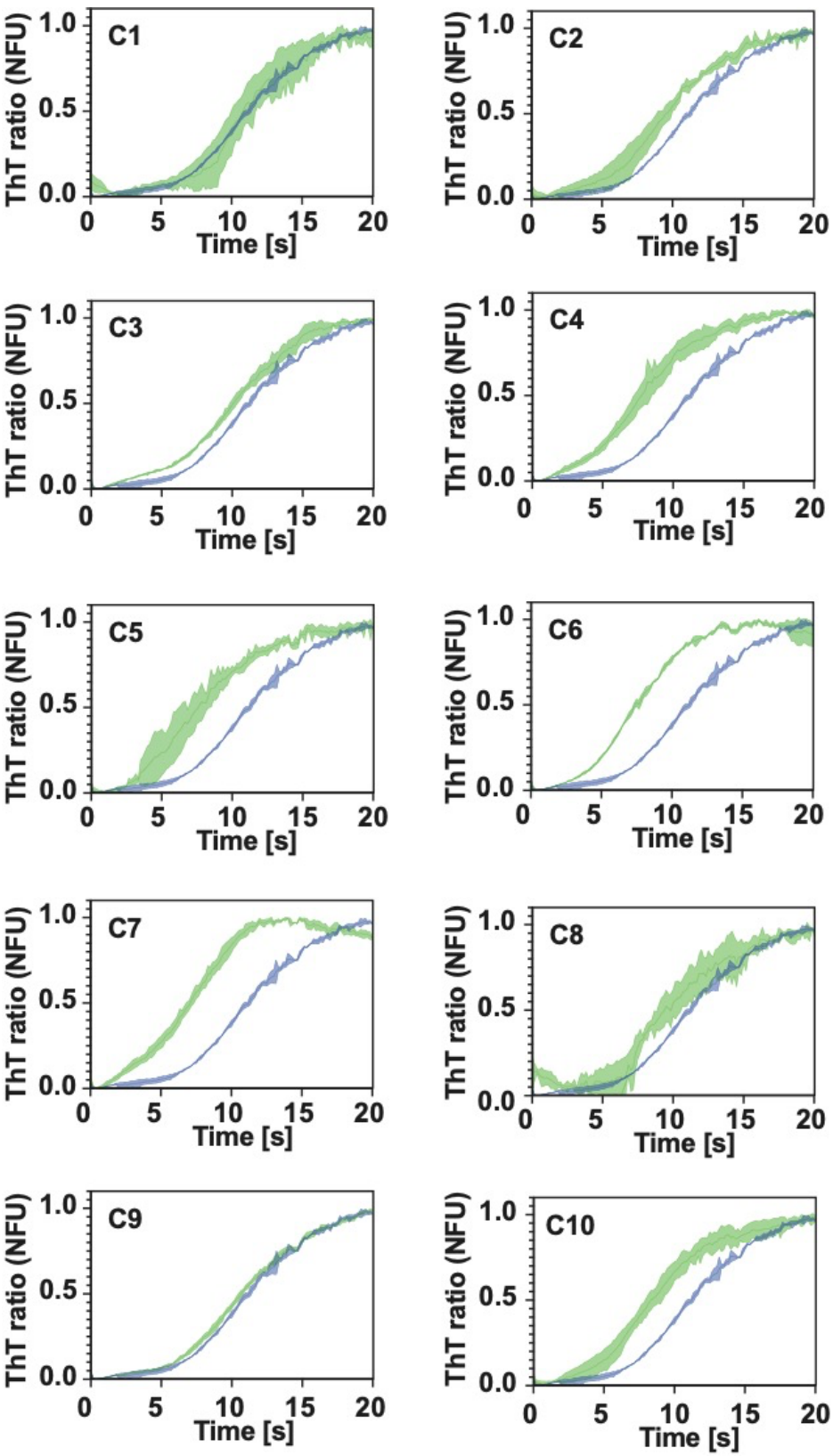

Supplementary Figure 3. Aggregation kinetics of Aβ42 incubated with different bacterial amyloid cores. The blue curve represents Aβ42 aggregation without any seeding. The green curve represents Aβ42 aggregation in the presence of pre-formed aggregates of the corresponding bacterial amyloid core. Each kinetic was performed using three biological replicates, with three technical replicates per biological replicate.

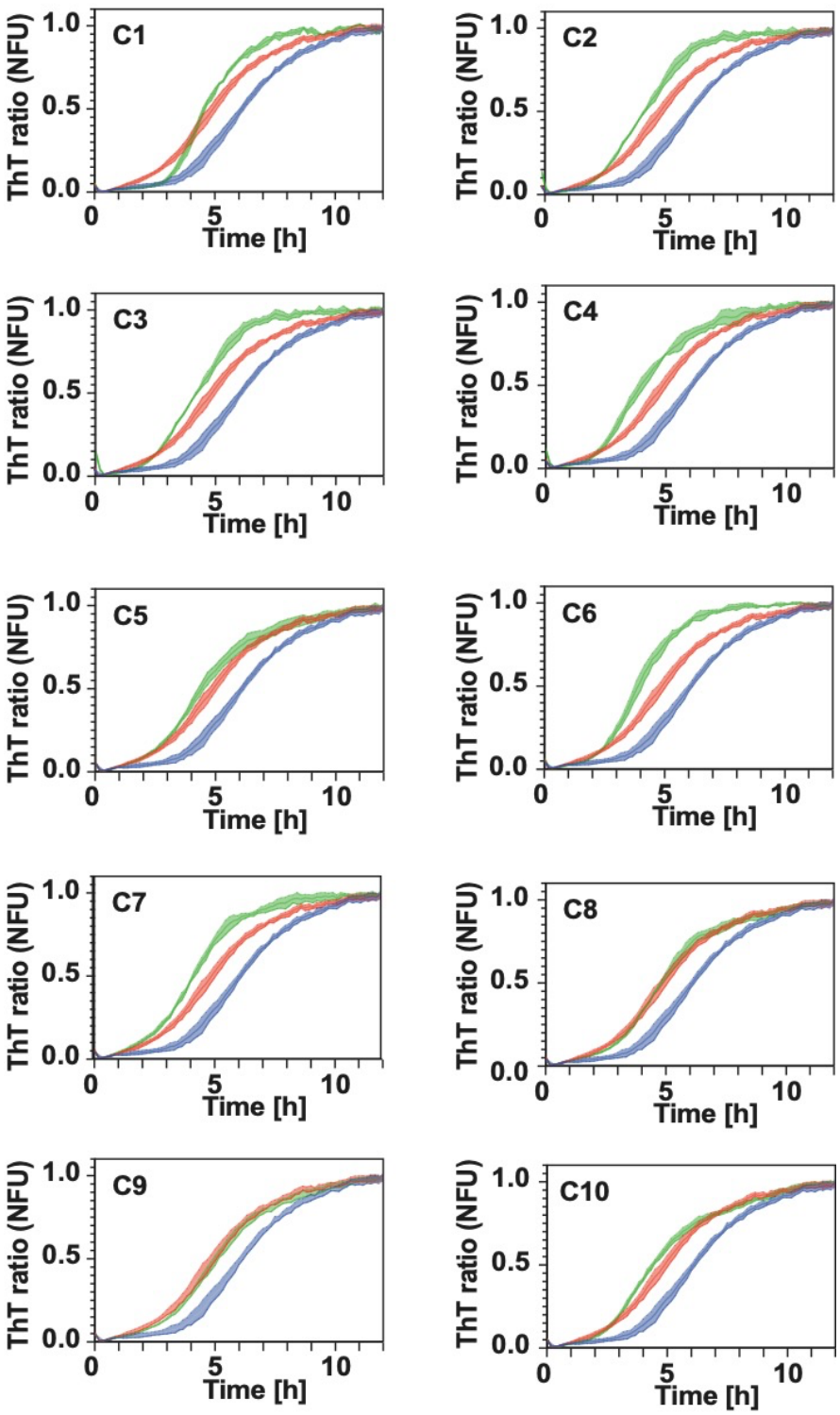

Supplementary Figure 4. Aggregation kinetics of Aβ42 incubated with different seeds of Aβ42. The blue curve represents Aβ42 aggregation without any seeding. The red curve represents Aβ42 aggregation in the presence of pure Aβ42 aggregates The green curve represents Aβ42 aggregation in the presence of the Aβ42 aggregates formed in the presence of the corresponding bacterial amyloid core. Each kinetic was performed using three biological replicates, with three technical replicates per biological replicate.

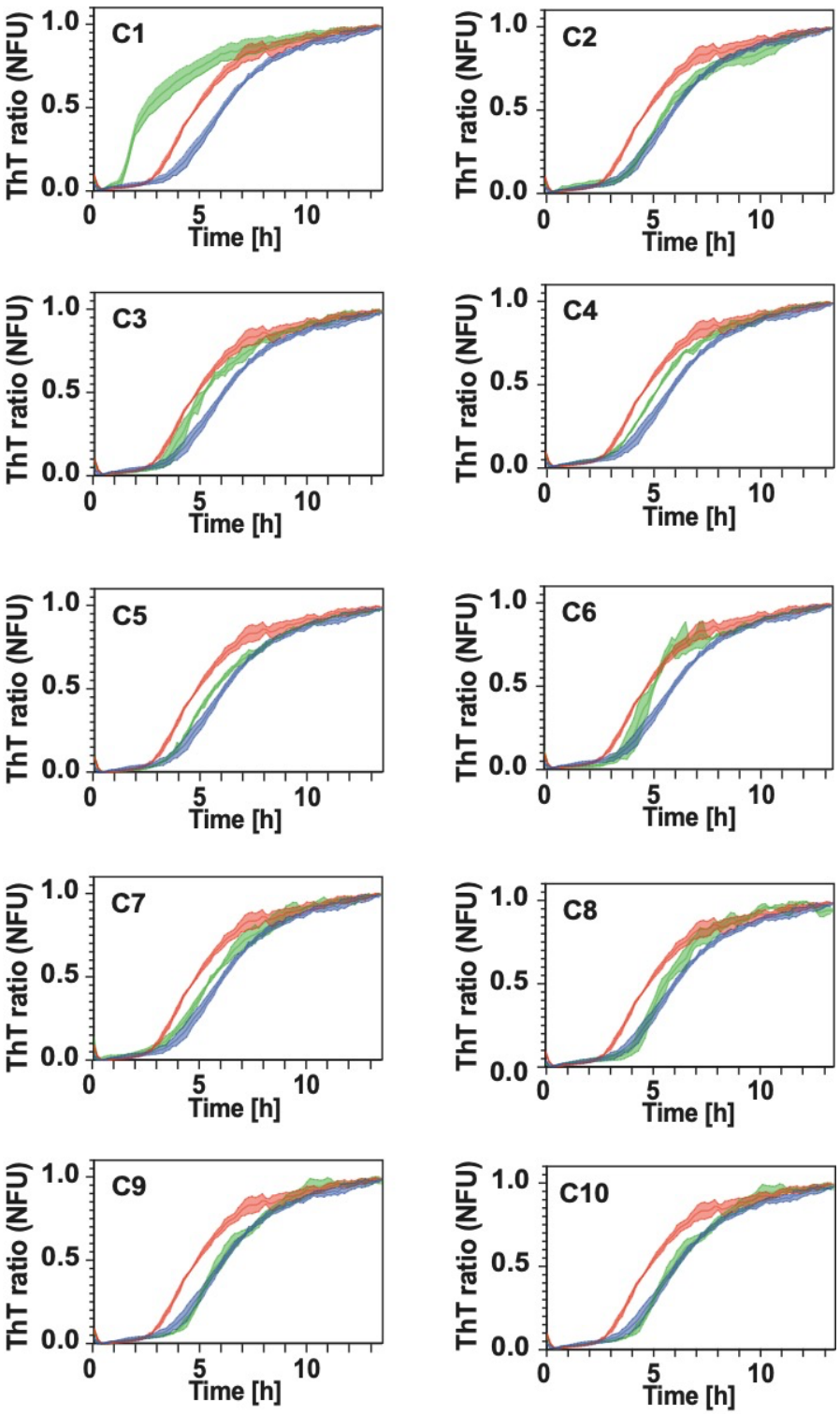

Supplementary Figure 5. Aggregation kinetics of Aβ42 incubated with different seeds of Aβ40. The blue curve represents Aβ42 aggregation without any seeding. The red curve represents Aβ42 aggregation in the presence of pure Aβ40 aggregates The green curve represents Aβ42 aggregation in the presence of the Aβ40 aggregates formed in the presence of the corresponding bacterial amyloid core. Each kinetic was performed using three biological replicates, with three technical replicates per biological replicate.